the FEBS Journal

Structure determination and biochemical studies on *Bacillus stearothermophilus* E53Q serine hydroxymethyltransferase and its complexes provide insights on function and enzyme memory

V. Rajaram[1]*, B. S. Bhavani[3]*, Purnima Kaul[3], V. Prakash[3], N. Appaji Rao[2], H. S. Savithri[2] and M. R. N. Murthy[1]

1 Molecular Biophysics Unit, Indian Institute of Science, Bangalore, India
2 Department of Biochemistry, Indian Institute of Science, Bangalore, India
3 Department of Protein Chemistry and Technology, Central Food Technological Research Institute, Mysore, India

Keywords
crystal structure; enzyme memory; pyridoxal 5′-phosphate; SHMT

Correspondence
M. R. N. Murthy, Molecular Biophysics Unit, Indian Institute of Science, Bangalore 560 012, India
Fax: +91 80 2360 0535
Tel: +91 80 2293 2458
E-mail: mrn@mbu.iisc.ernet.in

*These authors contributed equally to this work

(Received 4 March 2007, revised 6 May 2007, accepted 14 June 2007)

doi:10.1111/j.1742-4658.2007.05943.x

Serine hydroxymethyltransferase (SHMT) belongs to the α-family of pyridoxal 5′-phosphate-dependent enzymes and catalyzes the reversible conversion of L-Ser and tetrahydrofolate to Gly and 5,10-methylene tetrahydrofolate. 5,10-Methylene tetrahydrofolate serves as a source of one-carbon fragment in many biological processes. SHMT also catalyzes the tetrahydrofolate-independent conversion of L-*allo*-Thr to Gly and acetaldehyde. The crystal structure of *Bacillus stearothermophilus* SHMT (bsSHMT) suggested that E53 interacts with the substrate, L-Ser and tetrahydrofolate. To elucidate the role of E53, it was mutated to Q and structural and biochemical studies were carried out with the mutant enzyme. The internal aldimine structure of E53QbsSHMT was similar to that of the wild-type enzyme, except for significant changes at Q53, Y60 and Y61. The carboxyl of Gly and side chain of L-Ser were in two conformations in the respective external aldimine structures. The mutant enzyme was completely inactive for tetrahydrofolate-dependent cleavage of L-Ser, whereas there was a 1.5-fold increase in the rate of tetrahydrofolate-independent reaction with L-*allo*-Thr. The results obtained from these studies suggest that E53 plays an essential role in tetrahydrofolate/5-formyl tetrahydrofolate binding and in the proper positioning of Cβ of L-Ser for direct attack by N5 of tetrahydrofolate. Most interestingly, the structure of the complex obtained by cocrystallization of E53QbsSHMT with Gly and 5-formyl tetrahydrofolate revealed the gem-diamine form of pyridoxal 5′-phosphate bound to Gly and active site Lys. However, density for 5-formyl tetrahydrofolate was not observed. Gly carboxylate was in a single conformation, whereas pyridoxal 5′-phosphate had two distinct conformations. The differences between the structures of this complex and Gly external aldimine suggest that the changes induced by initial binding of 5-formyl tetrahydrofolate are retained even though 5-formyl tetrahydrofolate is absent in the final structure. Spectral studies carried out with this mutant enzyme also suggest that 5-formyl tetrahydrofolate binds to the E53QbsSHMT-Gly complex forming a quinonoid intermediate and falls off

Abbreviations
bsSHMT, *Bacillus stearothermophilus* SHMT; CD, circular dichroic; eSHMT, *Escherichia coli* SHMT; FTHF, 5-formyl THF; IPTG, isopropyl thio-β-D-galactoside; mcSHMT, murine cytosolic SHMT; LB, Luria–Bertani; PLP, pyridoxal 5′-phosphate; rcSHMT, rabbit liver cytosolic SHMT; scSHMT, sheep liver cytosolic SHMT; SHMT, serine hydroxymethyltransferase; THF, tetrahydrofolate.

within 4 h of dialysis, leaving behind the mutant enzyme in the gem-diamine form. This is the first report to provide direct evidence for enzyme memory based on the crystal structure of enzyme complexes.

Serine hydroxymethyltransferase (SHMT) is a member of the α-family of pyridoxal 5′-phosphate (PLP)-dependent enzymes [1]. It catalyzes the reversible interconversion of L-Ser and tetrahydrofolate (THF) to Gly and 5,10-methylene THF (5,10-CH_2THF). This compound serves as a key intermediate in the biosynthesis of methionine, thymidylate, purines, formyl t-RNA and a variety of other end products that require one-carbon fragments for their synthesis [2]. Increase in the activity of SHMT along with enhanced DNA synthesis in neoplastic tissues has suggested that SHMT might be a target for cancer chemotherapy [3]. In addition to its physiological reaction, SHMT catalyses the aldol cleavage of a number of β-hydroxy amino acids such as L-Thr, L-*allo*-Thr, L-*threo*- and L-*erythro*-β-phenyl serine [4–6]. It also catalyzes transamination, racemization and decarboxylation reactions [7].

SHMT has been isolated and studied from several sources. X-ray crystal structures of SHMT from human liver (hc) [8], murine (mc) [9], rabbit liver (rc) [10], *Escherichia coli* (e) [11] and *Bacillus stearothermophilus* (bs) [12] have been determined. The enzyme from prokaryotes is a dimer, whereas that from eukaryotic organisms is a dimer of tight dimers. It was suggested that SHMT cleaves L-Ser to Gly and formaldehyde by a retroaldol mechanism, in which the cleavage is initiated by abstraction of the hydroxy proton of L-Ser by a base at the active site. The formaldehyde generated interacts with THF to form 5,10-CH_2THF, which is released from the active site. Gly dissociates from the active site in a rate-determining step to complete the catalytic cycle [13]. Of the two groups that could serve as bases for abstracting proton (E53 and H122 in bsSHMT), E53 was present in its protonated form in the crystal structure, suggesting that it could not be involved in the proton abstraction step of catalysis [11,12]. Mutation of the other residue, H147 in scSHMT corresponding to H122 in bsSHMT, led only to a partial loss of enzyme activity, indicating that it could not be the residue abstracting the proton [14]. In addition, to abstract the proton from CH_2OH of L-Ser, an antiperiplanar geometry of the atoms involved in the electron movement is required. However, the crystal structure of serine external aldimine of bsSHMT suggests that the geometry is not optimal for retroaldol cleavage. Therefore, a direct transfer mechanism was suggested for the reaction catalyzed by SHMT [12]. This proposal envisages direct nucleophilic attack on the Cβ carbon of L-Ser by N5 of THF leading to the formation of a covalent adduct of THF and serine. In their revised mechanism, Szebenyi *et al.* [15] also proposed that there is a direct nucleophilic attack by N5 of THF on Cβ of L-Ser leading to Cα–Cβ bond cleavage to form 5,10-CH_2THF and glycine bound anion. It was noted that, in the reverse reaction, the N5 atom of THF is not optimally positioned for S_N2 nucleophilic substitution of the serine hydroxyl. To resolve these difficulties, Szebenyi *et al.* [15] determined the structures of E75Q and E75L mutants of rcSHMT and studied their properties. However, the structures determined by them were not at high resolution and suffered from a lack of order in the bound amino acids [15]. In an effort to resolve this ambiguity, we determined the structure of E53QbsSHMT and its binary complexes with Gly, L-Ser, L-*allo*-Thr and ternary complex with Gly and 5-formyl-THF (FTHF). In addition, the biochemical and spectral properties of these complexes were examined. Mutation of E53 to Q weakens the binding of THF/FTHF to the Gly binary complex. The results highlight the role of E53 in binding of THF/FTHF and in the proper positioning of L-Ser for direct attack by N5 of THF.

The structure of E53QbsSHMT in the presence of Gly and FTHF shows changes in the position of the active site residues that are reminiscent of FTHF binding to bsSHMT even though electron density for FTHF was not traceable. The differences in the structure of the E53QbsSHMT-Gly binary complex and the structure obtained in the presence of Gly and FTHF provide direct evidence to suggest that the complex retains the orientation of PLP (gem-diamine), which was seen in the crystal structure of bsSHMT-Gly-FTHF ternary complex even in the absence of bound FTHF [12]. This is an example of 'enzyme memory' seen for the first time in crystal structure.

Results and Discussion

E53QbsSHMT internal aldimine

The overall structure of E53QbsSHMT internal aldimine is very similar to that of bsSHMT. The rmsd of the corresponding Cα atoms upon superposition of the

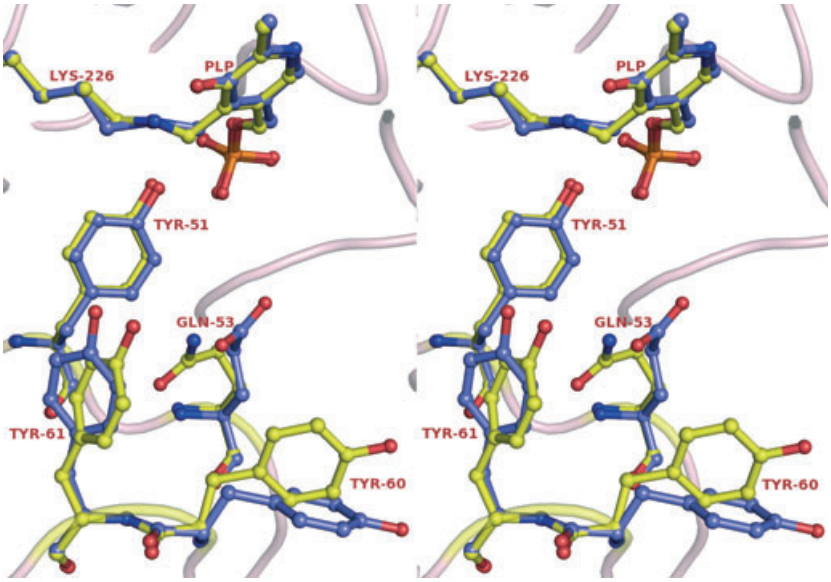

Fig. 1. Conformation of residues Y51, E53, Y60, Y61 and Schiff base (PLP covalently linked to K226) in E53QbsSHMT mutant (Yellow) with respect to bsSHMT (Blue). Y51 and the Schiff base are in the same orientation in E53QbsSHMT and bsSHMT, whereas the orientations of E53, Y60 and Y61 have changed.

wild-type and mutant structures is 0.10 Å. The orientation of PLP in E53QbsSHMT is identical to that of bsSHMT [12]. The most obvious differences are seen in and around the mutated residue E53. The side chain of Q53 in E53QbsSHMT is in a different conformation compared to that of E53 in bsSHMT. Changes are also observed in two adjacent Tyr residues 60 and 61. The plane of phenyl ring of Y60 in E53QbsSHMT is almost perpendicular to that observed in bsSHMT. In comparison, the shift is less in the case of Y61 (approximately 18°) (Fig. 1). The absorption spectrum of E53QbsSHMT shows a λ_{max} at 425 nm similar to that of bsSHMT [16].

E53QbsSHMT-Gly external aldimine

In the Gly and Ser external aldimine complexes of E75Q and E75LrcSHMT, the electron density for the ligands was not well defined [15]. In contrast, excellent electron density was observed for the ligands in E53QbsSHMT. The Gly external aldimine of E53QbsSHMT (E53QbsSHMT-Gly) shows rmsd of 0.14 Å with respect to Gly external aldimine of bsSHMT (bsSHMT-Gly) considering all Cα atoms for superposition. The side chain conformation of Q53 in E53QbsSHMT-Gly is only marginally different from that seen for E53 in bsSHMT-Gly. Unlike in the internal aldimine, smaller differences are observed in the conformation of the residues Y60 and Y61. In bsSHMT-Gly, the plane of the PLP ring is rotated by 24 ° compared to internal aldimine; an identical change in orientation of PLP was observed in the case of E53QbsSHMT-Gly.

The most significant difference in the structure is observed in the case of the bound Gly. The carboxylate group of Gly is in two distinct conformations in E53QbsSHMT-Gly. In one conformation, the carboxylate group forms hydrogen bonds with R357, as in bsSHMT-Gly [12]. In the second conformation, the carboxylate forms hydrogen bonds with NE2 of Q53 (3.34 Å) and NE2 of H122 (3.32 Å). This second conformation has an occupancy of 0.4. When the carboxylate is in the conformation found more predominantly (i.e. towards R357), a water molecule with an occupancy of 0.6 is present close to the position corresponding to the second conformation of the carboxylate group (Fig. 2A,B). The hydrogen bonding between Q53 and the second conformation of carboxylate of Gly found in E53QbsSHMT-Gly is less likely to occur in the wild-type enzyme. The water molecule with partial occupancy is stabilized by its interaction with OG of S172 (3.2 Å) and another water molecule (2.76 Å). Apart from the above differences, there is also a small movement (0.2–0.4 Å) of the main chain in the region 385–394. This region is solvent exposed and is not near the active site or near the site of mutation.

E53QbsSHMT in presence of Gly and FTHF

Addition of Gly to the mutant enzyme showed a small decrease in the absorption at 425 nm and a corresponding increase at 495 nm, indicating the presence of small amount of quinonoid intermediate. The formation of the quinonoid intermediate requires abstraction of a proton from the α-carbon atom of the bound

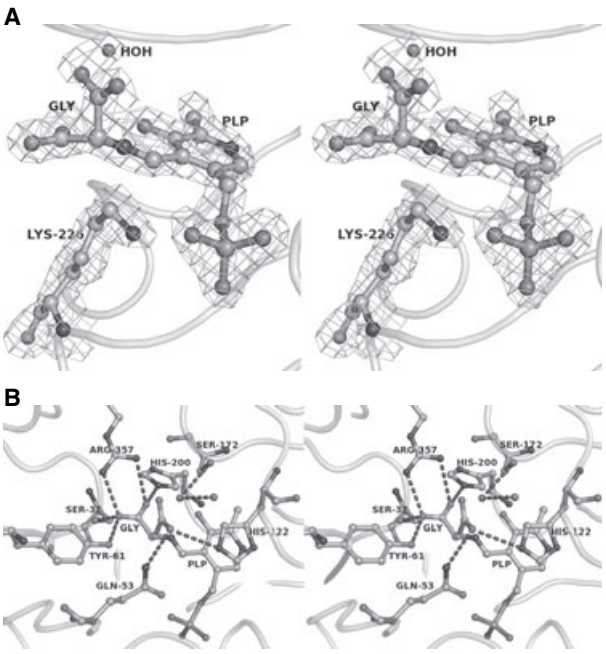

Fig. 2. (A) Stereo diagram illustrating electron density (omit map) corresponding to PLP and Gly in E53QbsSHMT-Gly. The two conformations of Gly are shown. A water molecule is present close to the second conformation of Gly with an occupancy of 0.6. (B) Stereo diagram showing the interactions (dotted lines) of carboxyl group of Gly with other residues in the E53QbsSHMT-Gly complex.

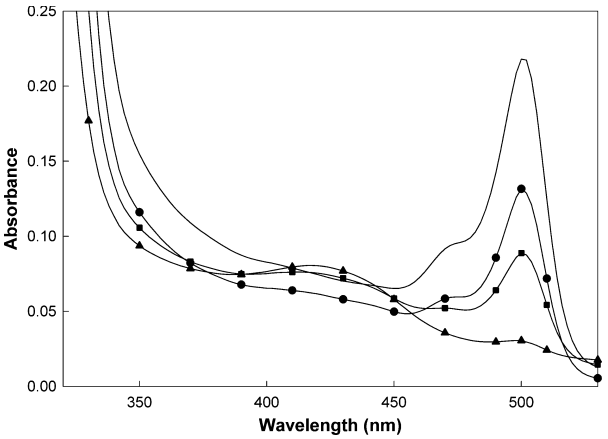

Fig. 3. Time course of disappearance of quinonoid intermediate in E53QbsSHMT. The spectrum of bsSHMT-Gly-FTHF (1 mg·mL^{-1} enzyme, 50 mM Gly, 500 μM FTHF) and E53QbsSHMT-Gly(FTHF) had absorbance maximum at 500 nm, suggesting the presence of quinonoid intermediate (–). Spectra recorded after (●) 1, (■) 2 and (▲) 3 h of dialysis, respectively. A significant decrease was observed in the quinonoid intermediate peak (500 nm) with concomitant appearance of a peak at 425 nm (▲). bsSHMT quinonoid intermediate peak at 500 nm was unchanged after dialysis for 4 h (–).

Gly. Further addition of THF or FTHF increased the absorbance significantly at 495 nm and 500 nm, respectively (Fig. 3), suggesting conversion of a significant fraction of the enzyme to the quinonoid form. A similar observation has been made with the wild-type enzyme [16].

Intriguing results are obtained with the structure of the mutant enzyme determined in the presence of Gly and FTHF [E53QbsSHMT-Gly(FTHF)] In the wild-type enzyme, these ligands form a ternary complex (bsSHMT-Gly-FTHF). In contrast to the orthorhombic space group with a monomer in the asymmetric unit of bsSHMT internal and external aldimines, the ternary complex crystallizes in a monoclinic cell with β angle very close to 90° and a dimer in the asymmetric unit due to asymmetric binding of FTHF to the two subunits, which leads to breakdown of the two-fold symmetry and hence to the monoclinic crystal form [12]. Attempts to crystallize E53QbsSHMT in the presence of Gly and FTHF yielded orthorhombic crystals and the density for FTHF could not be traced. PLP in this complex was trapped in a gem-diamine form covalently bonded to both the active site lysine and the added Gly amino group (Fig. 4A). Gem-diamine is an intermediate formed in the interconversion of the enzyme between internal and external aldimine forms. The orientation of PLP in E53QbsSHMT-Gly(FTHF) complex is closer to that of bsSHMT-Gly-FTHF than its orientation in the internal or external aldimine structures of mutant or wild-type enzymes. This is consistent with the earlier observation that the orientation of PLP in the ternary complex of mcSHMT [9] is similar to the PLP in the gem-diamine form. However, the present structure does not contain density for FTHF. The similarity in the orientation of PLP to that of the wild-type ternary complex [12] and absence of FTHF in the crystal structure suggests that there is an initial binding of FTHF leading to an alteration in the orientation of PLP and, subsequently, FTHF falls off from the active site. The differences between the structures of this complex and Gly external aldimine suggest that the changes induced by initial binding of FTHF are retained, even though FTHF is absent from the final structure.

Another interesting observation in the structure of E53QbsSHMT-Gly(FTHF) is that the phosphate group of PLP is in two conformations (Fig. 4A,B). The interactions in the first conformation are similar to those described for the bsSHMT-Gly-FTHF [12]. The second conformation is stabilized mainly by hydrogen bonding to atoms from the symmetry related subunit. One of the phosphate oxygen atoms in this

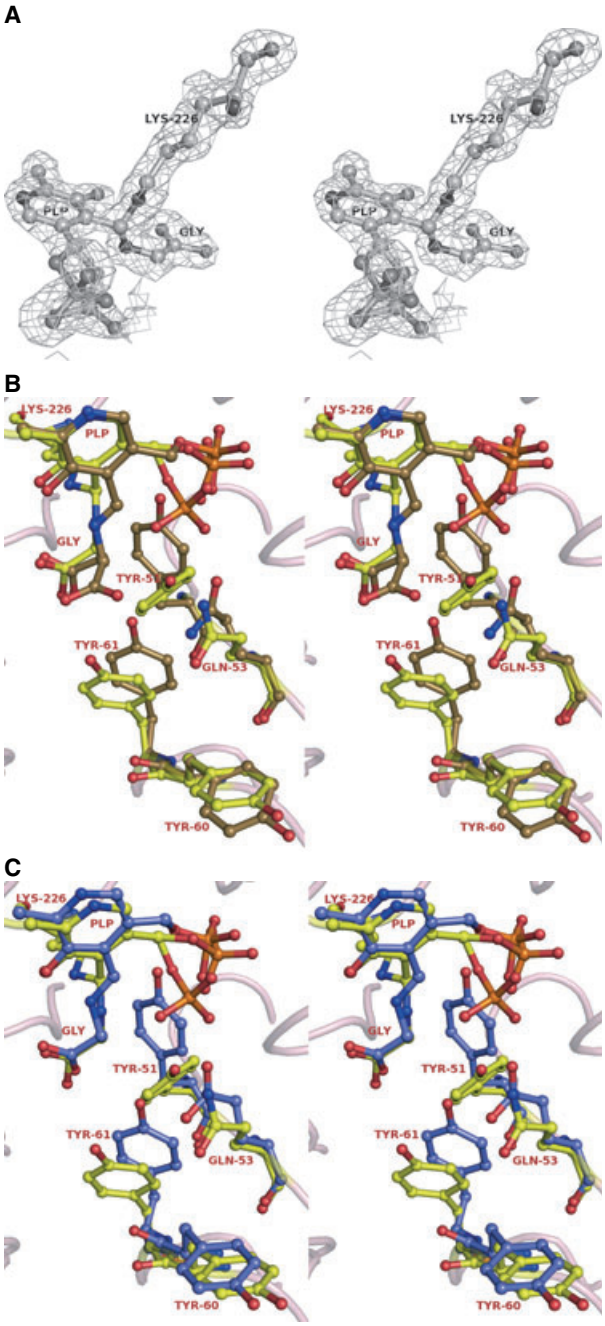

Fig. 4. (A) Electron density (omit map) showing gem-diamine in E53QbsSHMT-Gly-FTHF complex. (B) Superposition of residues Y51, E53, Y60 and PLP in E53QbsSHMT-Gly(FTHF) (yellow) and E53QbsSHMT-Gly (brown). (C) Superposition of residues Y51, E53, Y60 and PLP in E53QbsSHMT-Gly(FTHF) (yellow) and bsSHMT-Gly-FTHF (blue).

conformation is held by hydrogen bonding interaction with the phenolate oxygen of Y51, N of G257 and NE2 of Q53 of the symmetry related subunit. Another oxygen atom is held by hydrogen bonding to NE2 of H122 and phenolate oxygen of Y51 of the symmetry related subunit. The third oxygen is hydrogen bonded to a water molecule and NE2 of H122. The new position of the phosphate group induces a displacement in Y51. As Y51 moves to the position occupied earlier by Y61, a corresponding movement is also found in Y61 (Fig. 4B). In all other complexes of E53QbsSHMT, OH of Y51 interacts with OP2 of PLP (Fig. 4B,C). As the orientation of Y51 is different in this complex, a water molecule compensates for this interaction. There are also small main chain movements in the regions 83–87, 237–244, 255–258 and 385–394. Most of these regions are solvent exposed and are not directly related to the active site or site of mutation. The overall structure (other than the changes described above) of E53QbsSHMT-Gly(FTHF) matches better with bsSHMT-Gly (rmsd = 0.15 Å) than with the A or B subunits of bsSHMT-Gly-FTHF with which it has rmsd of 0.41 and 0.44 Å, respectively.

Upon the addition of FTHF to the binary complex of E53QbsSHMT-Gly, the color of the solution changed from yellow to pink, indicating the formation of a quinonoid intermediate. However by the time crystals were formed, the color of the drop had turned yellow, suggesting the conversion of the quinonoid intermediate to other forms of the enzyme. Crystallographic results suggest that the final state of the enzyme is influenced by the initial binding of FTHF and differs significantly from the binary complex formed in the absence of FTHF.

Spectroscopic observations also suggest that FTHF dissociates from the enzyme upon prolonged storage (12 h). The rate of formation of the quinonoid intermediate upon addition of THF to the mutant enzyme-Gly complex was 2.2 s^{-1} as determined by stopped flow kinetics, compared to 340 s^{-1} for bsSHMT. It can be recalled that the formyl oxygen group of FTHF interacts with E53 in bsSHMT-Gly-FTHF ternary complex [12]. Both bsSHMT and E53QbsSHMT ternary complexes were dialyzed against buffer (50 mM potassium phosphate pH 7.4 containing 1 mM EDTA and 1 mM 2-mercaptoethanol) devoid of Gly and FTHF and spectra were recorded at intervals of 1 h. Significant decrease was observed in the quinonoid intermediate peak (500 nm) with concomitant appearance of a peak at 425 nm (Fig. 3) at the end of 4 h, suggesting that FTHF had dissociated from the complex and distribution of the intermediates was altered in the case of the E53QbsSHMT ternary complex. On the other hand, the bsSHMT quinonoid intermediate peak at 500 nm did not change after dialyzing for 4 h (Fig. 3). PLP was estimated in the dialyzed sample and it was found that the amount (1 mol of PLP per mol

of subunit) was the same in both bsSHMT and E53QbsSHMT. The dissociation constant (K_d) of FTHF for E53QbsSHMT-Gly was determined from double reciprocal plots of the change in the absorbance at 500 nm versus FTHF concentration at different fixed concentrations of Gly. A replot of the Y intercept versus concentration of Gly gave the K_d values for FTHF. A similar experimental approach was used to determine the K_d in the case of rcSHMT [17]. The K_d value for E53QbsSHMT-Gly was 25 μM compared to 10 μM for bsSHMT-Gly. The 2.5-fold higher K_d further suggests that the affinity of E53QbsSHMT-Gly for FTHF is reduced. Although the density for FTHF is not seen in E53QbsSHMT-Gly(FTHF), the orientation of PLP (gem-diamine form) in this complex is very similar to that of wild-type ternary complex [12]. The circular dichroic (CD) spectrum of E53QbsSHMT in the presence of Gly and FTHF showed a band at 343 nm (Fig. 5), suggesting the presence of the gem-diamine form of E53QbsSHMT. The crystal structure of E53Q-Gly(FTHF) also showed that PLP is indeed in the gem-diamine form and the FTHF is not bound (Fig. 4A). This is an interesting case of 'enzyme memory'. One of the important kinetic evidences for the occurrence of enzyme memory is the demonstration of significant variation of acceptor double reciprocal slopes with variation in donor substrate. In the case of ascorbate oxidase, changes in the slope in the double reciprocal plot with three different donor substrate have been used to demonstrate enzyme memory [18]. In order to show that indeed

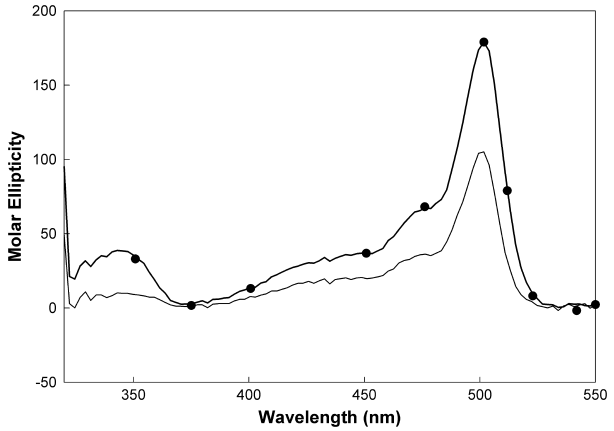

Fig. 5. Visible CD spectra of bsSHMT-Gly-FTHF (1 mg·mL^{-1} enzyme, 50 mM Gly, 500 μM FTHF) and E53QbsSHMT-Gly(FTHF). The CD spectrum of the ternary complex of the E53QbsSHMT has significant ellipticity at 343 nm, suggesting the presence of gem-diamine (●); ternary complex of bsSHMT shows only quinonoid intermediate (–).

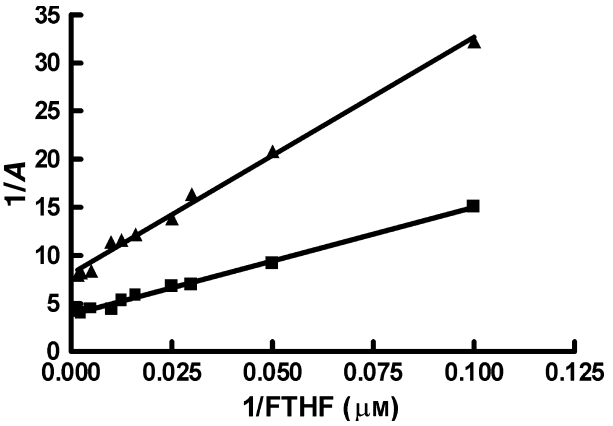

Fig. 6. Double reciprocal plots for the formation of quinonoid intermediate before and after dialysis of E53QbsSHMT-Gly(FTHF). The enzyme (1 mg·mL^{-1}) was incubated with 10 mM glycine and a varying concentration of FTHF (0–400 μM), for 1 min and absorbance at 500 nm was measured. The reciprocal of A_{500} was plotted against the reciprocal of FTHF concentration (■). The enzyme (10 mg) was incubated with 10 mM glycine and 500 μM FTHF for 5 min and then dialyzed against buffer D not containing glycine and FTHF. Such an enzyme was once again incubated with glycine (10 mM) and different concentrations of FTHF as in (■) and the absorbance was measured at 500 nm. The double reciprocal plot ($1/A$ versus $1/$[FTHF]) for the dialyzed enzyme is shown (▲).

E53QbsSHMT-Gly(FTHF) is kinetically different from E53QbsSHMT-Gly, we carried out overnight dialysis of E53QbsSHMT-Gly(FTHF) against the buffer not containing glycine and FTHF and determined the slope for the formation of quinonoid intermediate by the addition of 10 mM glycine and varying FTHF concentrations. As shown in Fig. 6 the double reciprocal plot for the formation of quinonoid intermediate as a function of FTHF concentration is different for E53QbsSHMT before and after exposure to glycine and FTHF. The two forms of enzymes bind to FTHF with different slopes (before dialysis −104.4; after dialysis −234.1). In contrast, for bsSHMT, slopes were similar before (21.42) and after dialysis (33.74). If the lines were parallel then it would suggest that E53QbsSHMT has no enzyme memory and that the two forms before and after dialysis are kinetically similar. However, because the slopes are drastically different for E53QbsSHMT, it suggests that the enzyme conformation previously exposed to glycine and FTHF is different from that before exposure and that E53QbsSHMT exhibits enzyme memory. The slow conformational change seen in the E53QbsSHMT and not in the bsSHMT enzyme highlights the importance of glutamate residue in enhanced cleavage of L-Ser in the presence of THF.

It is possible to imagine a series of reasonable atomic movements that account for the observed differences between the complexes of E53QbsSHMT-Gly obtained in the absence and presence of FTHF. The carboxylate of Gly is in a single conformation in the wild-type enzyme in which it is hydrogen bonded to R357. In contrast, in E53QbsSHMT, it is partitioned between two positions that allow hydrogen bonding with Q53 and R357, respectively. Upon FTHF binding, the Gly carboxylate, which is hydrogen bonded with E53, is in severe short contact with the aldehyde group of FTHF and hence is confined to a single position that allows bonding with only R357, a situation similar to the wild-type enzyme. To compensate for the loss of hydrogen bonding interaction with the carboxylate, Q53 pulls the phosphate of PLP into an alternate position suitable for bonding. These rearrangements of atoms probably lead to dissociation of FTHF. However, the alternate position occupied by phosphate does not return to its original position, probably resulting in PLP in the gem-diamine form (Figs 3Aand 4A) [19–22].

E53QbsSHMT-Ser external aldimine

The structure of E53QbsSHMT complexed with L-Ser (E53QbsSHMT-Ser) shows an rmsd of 0.11 Å with respect to that of bsSHMT-Ser. The side chain conformations of Q53 in the mutant and bsSHMT-Ser complexes are similar except for OE1 and NE2 atoms. No significant changes in the conformation of residues Y60, Y61 and PLP orientation are observed in the mutant with respect to bsSHMT-Ser. However, the side chain hydroxyl of bound serine is in two positions. The first position is identical to that of bsSHMT-Ser complex. In the second position, Ser-OG has a weak hydrogen bonding interaction with OG of S172 (3.59 Å) and a water molecule (3.46 Å). Apart from these changes near the active site, a small movement of the main chain is also observed in some solvent exposed regions such as 83–87 (0.2–0.4 Å) and 237–242 (0.4–0.7 Å).

Attempts to obtain crystals of ternary complex of bsSHMT and E53QbsSHMT in the presence of L-Ser and FTHF yielded only crystals of L-Ser external aldimine. Earlier attempts to obtain crystals of ternary complexes of bsSHMT and rcSHMT were also unsuccessful. The reason for this is thought to be the clash in the position of -CH_2OH of L-Ser and the formyl group of FTHF [12].

Mutation of E53 to Q led to a complete loss of THF-dependent cleavage of L-Ser. (Table 1). K_m and V_{max} of the mutant enzyme with L-Ser could not be determined because the activity was barely measurable even when the protein concentration was increased by 1000-fold. The direct displacement mechanism for L-Ser cleavage in the presence of THF envisages simultaneous attack by the N5 of THF on the Cβ of L-Ser and a proton transfer to the serine hydroxyl group, leading to the release of a water molecule. E53 in its protonated state is ideally situated for proton transfer because the distance of OG of E53 to the OH of L-Ser is 2.5 Å. Following this cleavage, Gly quinonoid intermediate is formed. The conversion of the Gly quinonoid intermediate to the external aldimine involves another protonation step. The Y61 OH group is at a distance of 2.95 Å from the α-carbon atom of Gly and appears to be suitable for this proton transfer. As the internal and external aldimines of SHMTs have similar visible absorbance spectrum, CD studies were carried out to examine the formation of external aldamine. Addition of L-Ser causes a significant decrease in the molar ellipticity of bsSHMT at 425 nm (Fig. 7,

Table 1. Kinetic constants for bsSHMT and E53QbsSHMT. Specific activity is μmol of HCHO $min^{-1}{\cdot}mg^{-1}$ when L-Ser and THF were used as substrates and μmol of NADH oxidized $min^{-1}{\cdot}mg^{-1}$ with L-*allo*-Thr as substrate.

	Specific activity (L-Ser)		K_m (mM)		Specific activity
Enzyme	+ THF	– THF	L-Ser	L-*allo*-Thr	L-*allo*-Thr
bsSHMT	5.9	0.8×10^{-3}	0.9	0.8	0.645
E53QbsSHMT	0	1.5×10^{-3}	–	9.5	1.07

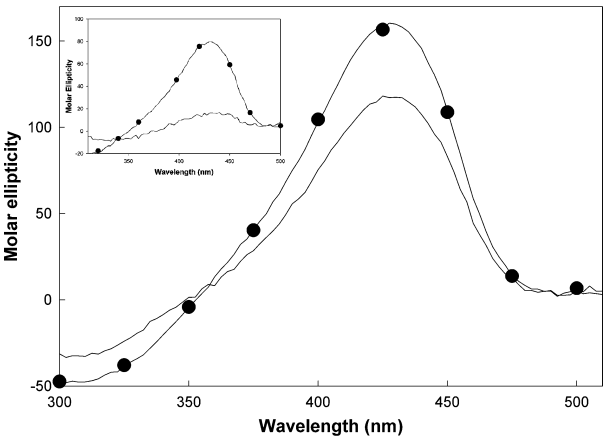

Fig. 7. Visible CD spectrum of E53QbsSHMT with L-Ser. The spectrum was recorded at a protein concentration of 1 $mg{\cdot}mL^{-1}$ in the range of 300–550 nm (●). Further addition of L-Ser (50 mM) to E53QbsSHMT caused a decrease in the ellipticity at 425 nm (–). Inset: Visible CD spectrum of bsSHMT (●) and bsSHMT with L-Ser (–).

inset). On the other hand, addition of L-Ser to E53QbsSHMT (Fig. 7) causes only a small change, suggesting that this external aldimine is spectrally different from that of the bsSHMT-Ser complex. This could be due to subtle changes at the active site environment upon mutation that result in the binding of serine with its hydroxyl group in two distinct orientations. It was observed that addition of L-Ser to bsSHMT caused an increase in thermal melting temperature (T_m) from 65 to 80 °C whereas, with the mutant enzyme, there was no change (72 °C). Addition of Gly had no effect on the T_m of either bsSHMT or E53QbsSHMT. These results suggest that the interactions of L-Ser with bsSHMT and E53QbsSHMT are significantly different. The results presented so far suggest that E53 is involved in the proper positioning of THF/FTHF and the Cβ carbon of serine, enabling direct nucleophilic attack in the forward reaction.

E53QbsSHMT and bsSHMT in presence of L-*allo*-threonine

Apart from folate-dependent interconversion of L-Ser and Gly, SHMT also catalyses the folate-independent conversion of L-*allo*-Thr to Gly and acetaldehyde. Attempts to crystallize bsSHMT and E53QbsSHMT in the presence of L-*allo*-Thr yielded crystals with only Gly bound to PLP. This observation suggested that L-*allo*-Thr was completely cleaved to Gly. The density for acetaldehyde formed in the cleavage was not seen in the crystal structure. E53QbsSHMT-*allo*-Thr and E53QbsSHMT-Gly structures superposed with an rmsd of 0.11 Å. In E53QbsSHMT-*allo*-Thr also, glycine carboxylate is in two conformations as in E53QbsSHMT-Gly. Cleavage of L-*allo*-Thr to Gly and acetaldehyde requires several proton transfers. It is likely that Y61, which undergoes large movements when the enzyme forms complexes with ligands, is involved in proton abstraction from the *allo*-Thr and/or the protonation of glycine quinonoid intermediate to the external aldimine.

The THF-independent activity with L-*allo*-Thr as substrate increased 1.5-fold upon E53Q mutation. It has been reported that the activity increases by four-fold in the case of E75QrcSHMT. The K_m and specific activity values for L-*allo*-Thr with bsSHMT were 0.8 mM and 0.65 μmol·mg^{-1}, respectively, and 9.5 mM and 1.1 μmol·mg^{-1}, respectively, with E53QbsSHMT. The increase in the activity with L-*allo*-Thr is consistent with the observation of only Gly bound at the active site when E53QbsSHMT was cocrystallized with L-*allo*-Thr.

Conclusions

The direct transfer mechanism envisages a direct attack of N5 of THF on the Cβ of L-Ser [12]. The role of E53 is to position the bound amino acid and THF for such an attack by suitable interactions with other active site residues. In addition, E53 also interacts with the formyl oxygen and N10 of FTHF. It is therefore not surprising that the mutation has affected the hydrogen-bonding network involving key residues such as Y60 and Y61 and the interaction with R357, which anchors the carboxyl group of the substrate. A consequence of these changes is the complete loss of THF-dependent physiological reaction with L-Ser. However THF-independent reaction is not reduced. The loss of interactions of the glutamate residue with the formyl oxygen and N10 of FTHF in the mutant enzyme weakens the interactions with THF/FTHF. Consequently, although a ternary complex is initially formed, FTHF dissociates and the mutant enzyme crystallizes in the gem-diamine form. These observations are reminiscent of enzyme memory observed in kinetic experiments with plant aspartate synthase, hexokinase and ascorbate oxidase [18–20]. The results on the formation of a quinonoid intermediate and gem-diamine complex and a slow dissociation of FTHF also indicate that E53QbsSHMT exhibits enzyme memory. This is the first instance of such a phenomenon observed in structural studies.

Experimental procedures

Materials

L-[3-^{14}C]-Serine, restriction endonucleases and DNA-modifying enzymes were obtained from Amersham Pharmacia Biotech Ltd (Little Chalfont, UK). Deep Vent Polymerase was purchased from New England Biolabs (Beverly, MA, USA). Taq DNA polymerase was purchased from Bangalore Genei Pvt. Ltd (Bangalore, India). DEAE-cellulose, Gly, L-Ser, 2-mercaptoethanol, folic acid, PLP, isopropyl thio-β-D-galactoside (IPTG) and EDTA were obtained from Sigma Chemical Co. (St Louis, MO, USA). All other chemicals used were of analytical grade.

Bacterial strains and growth conditions

Escherichia coli strain DH5α (BRL) was the recipient for all the plasmids used in subcloning. The BL21 (DE3) pLysS [23] strain was used for bacterial expression of pRSH (*B. stearothermophilus* SHMT gene cloned and over expressed in pRSET C vector). Mutant constructs were similarly overexpressed. Luria–Bertani (LB) medium or

terrific broth with 50 $\mu g \cdot mL^{-1}$ of ampicillin was used for growing *E. coli* cells harboring the plasmids [24].

DNA manipulations

Plasmids were prepared by the alkaline lysis procedure [24]. Preparation of competent cells and transformation were carried out by the method of Alexander [25]. DNA fragments were eluted with QIA quick gel extraction buffer (Qiagen, Valancia, CA, USA).

E53Q mutant of bsSHMT was constructed using the primers: E53Q (sense) 5′-CAAATACGCGCAAGGCTATCCG-3′ and E53Q (antisense) 5′-CGGATAGCCTTGCGCGTATTTG-3′. The underlined nucleotides define the mutation introduced. Primers were used on pRSH template to construct the mutant by PCR based sense-antisense primer method [24]. DNA sequencing using an ABI prism automated DNA sequencer (Applied Biosystems, Foster City, CA, USA) confirmed presence of the mutation and showed that no other changes were present.

Expression and purification of bsSHMT and E53QbsSHMT

The expression and purification of the wild-type (bsSHMT) and the mutant enzymes were carried out according to Jala *et al.* [16]. Briefly, pRSH-E53Q constructs were transformed into *E. coli* BL21 (DE3) pLysS cells. A single colony was grown at 30 °C in 50 mL of LB medium containing 50 $\mu g \cdot mL^{-1}$ ampicillin. These cells were inoculated into 1 L of terrific broth containing 50 $\mu g \cdot mL^{-1}$ ampicillin. After 3–4 h at 30 °C, cells were induced with 0.3 mM IPTG for 4–5 h. The cells were then harvested, resuspended in 60 mL of buffer A (50 mM potassium phosphate pH 7.4 containing 1 mM 2-mercaptoethanol, 1 mM EDTA and 100 μM PLP) and sonicated. The supernatant obtained by centrifugation at 15 000 ***g*** for 30 min (using a Sorvall Evolution™ RC Superspeed Refrigerated Centrifuge with SS-34 rotor, from Thermo Fisher Scientific, Asheville, NC, USA) was subjected to 0–65% ammonium sulfate precipitation. The pellet obtained by centrifugation was resuspended in 20–30 mL of buffer B (20 mM potassium phosphate pH 8.0 containing 1 mM 2-mercaptoethanol, 1 mM EDTA and 50 μM PLP) and dialyzed for 24 h against the same buffer (1 L with two changes). The dialyzed sample was loaded onto DEAE-cellulose previously equilibrated with buffer B. The column was washed with 500 mL of buffer B and the bound protein was eluted with 50 mL of buffer C (200 mM potassium phosphate pH 6.4 containing 1 mM EDTA, 1 mM 2-mercaptoethanol, 50 μM PLP). The eluted protein was precipitated at 65% ammonium sulfate saturation, and the pellet was resuspended in buffer D (50 mM potassium phosphate pH 7.4 containing 1 mM EDTA and 1 mM 2-mercaptoethanol) and dialyzed against the same buffer (2 L with two changes) for 24 h. The purified protein was homogenous when examined by SDS/PAGE. Protein was estimated by the Lowry procedure using BSA as the standard [26].

Crystallization, data collection and processing

For the purpose of crystallization, after the final ammonium sulfate precipitation, the enzyme was dissolved in 100 mM Hepes pH 7.5 with 0.2 mM EDTA and 5 mM 2-mercaptoethanol and washed with 200 mL of the same buffer by repeated dilution followed by concentration using Amicon centricon filters. Crystals of E53QbsSHMT mutant were obtained by mixing 4 μL of E53QbsSHMT (18 $mg \cdot mL^{-1}$) and 4 μL of reservoir solution containing 100 mM Hepes pH 7.5 with 0.2 mM EDTA, 5 mM 2-mercaptoethanol and 50% 2-methyl 2,4-pentanediol. Complexes of E53QbsSHMT with Gly, L-Ser, L-*allo*-Thr and Gly and FTHF were crystallized using the same condition with 10 mM of the specified ligand. These procedures were identical to those used for the crystallization of bsSHMT and its complexes [12]. For crystallization experiments with FTHF, the enzyme was initially incubated with 2 mM FTHF. The crystals were soaked in the mother liquor for a few seconds and flash frozen in a stream of nitrogen at 100 K for collecting data. X-ray diffraction data were collected using a Rigaku (Tokyo, Japan) RU-200 rotating-anode X-ray generator (Cu-Kα radiation) equipped with a MAR research (Hamburg, Germany) imaging-plate detector system. Denzo and Scalepack from the HKL2000 suite (HKL Research Inc., Charlottesville, VA, USA) were used for indexing, integration, data reduction and scaling [27]. Crystals of E53QbsSHMT and its complexes belonged to the $P2_12_12$ space group and contained one monomer in the asymmetric unit. Cell dimensions and details of data collection are shown in Table 2.

Structure solution and model building

The bsSHMT crystal structure (1KKJ) was used as the initial model for the refinement of structures of E53QbsSHMT. Before initiating the refinement, PLP and water molecules were removed from the model. The model was then subjected to rigid body refinement followed by restrained refinement using REFMAC5 from the CCP4 suite [28]. Five percent of unique reflections were used to monitor the progress of refinement by R_{free}. Visualization of the electron density map and model fitting were peformed using COOT [29]. Structure was validated using PROCHECK [30]. Figures were generated using the program PYMOL [31].

For the complexes of E53QbsSHMT with Gly, L-Ser and L-*allo*-Thr, bsSHMT-Gly external aldimine crystal structure (1KL1) was used as the initial model. The models of E53QbsSHMT–ligand complexes were further refined in the same manner as described above. ALIGN was used for the superposition of structures [32]. Differences between the structures were detected visually and by calculating distances

Table 2. Data collection statistics of E53QbsSHMT and its complexes. Values in parantheses correspond to highest resolution bin.

Ligand(s) used	None	Gly	L-Ser	L-*allo*-Thr	Gly + FTHF	L-Ser + FTHF
Space group	$P2_12_12$	$P2_12_12$	$P2_12_12$	$P2_12_12$	$P2_12_12$	$P2_12_12$
a (Å)	61.07	61.28	61.30	61.13	60.96	61.26
b (Å)	106.73	106.30	106.47	106.21	106.46	106.58
c (Å)	56.88	57.317	57.29	57.07	56.99	57.21
Resolution (Å)	2.0	1.86	1.80	2.3	1.86	1.7
Completion (%)	99.1(99.4)	99.2 (94.4)	99.6 (99.8)	99.1 (98.8)	98.8 (92.0)	99.8 (100)
R_{merge} (%)	7.1 (40.5)	6.3 (32.6)	7.2 (48.8)	9.7 (36.2)	4.7 (38.3)	3.3 (20.9)
Total reflections	282 282	304 348	488 647	342 345	346 889	442 833
Unique reflections	25 550	31 957	35 532	16 978	31 400	41 942
$<I>/<\sigma I>$	14.9 (2.7)	18.2 (4.0)	16.0 (2.7)	15.9 (4.7)	17.5 (3.2)	43.32 (5.7)
Wilson B ($Å^2$)	25.3	23.2	21.5	34.9	25.0	18.6

Table 3. Refinement statistics of E53QbsSHMT and its complexes.

Ligand(s) used	None	Gly	L-Ser	L-*allo*-Thr	Gly + FTHF	L-Ser + FTHF
Resolution range (Å)	30–2.0	29.44–1.86	27.03–1.80	29.37–2.30	27.01–1.86	27.08–1.7
Final *R* (%)	17.3	15.5	16.2	18.2	16.3	16.1
Free *R* (%)	21.6	20.1	19.6	23.3	20.7	19.5
rmsd bond (Å)	0.010	0.014	0.014	0.007	0.015	0.012
rmsd Angle (°)	1.214	1.341	1.364	1.022	1.427	1.269
rmsd Chiral ($Å^3$)	0.082	0.092	0.093	0.066	0.092	0.086
Number of protein atoms	3117	3119	3134	3117	3117	3139
Number of ligand atoms	23	38	37	33	38	40
Number of water molecules	251	440	398	219	288	425
Average B-factor ($Å^2$)	23.26	19.52	18.26	26.51	21.54	14.87
Protein atoms	22.72	17.91	16.84	26.23	20.71	13.29
Ligand atoms	28.95	26.35	30.39	31.57	33.00	33.76
Water molecules	29.46	30.30	28.34	29.79	29.00	24.77
ϕ/ψ plot (%)						
Mostly allowed	94.0	94.0	92.9	93.4	93.1	93.1
Allowed	4.9	4.9	6.0	5.4	5.7	5.7
Generously allowed	0.3	0.3	0.3	0.6	0.6	0.3
Disallowed	0.9	0.9	0.9	0.6	0.6	0.9

between corresponding atoms after structural superposition. The details of the refinement statistics and quality of the refined structure are given in Table 3. The F_o–F_c annealed omit map was calculated using the CNS refinement program [33] with a spherical omit region of 5 Å around PLP for E53QbsSHMT-Gly and E53QbsSHMT-Gly(FTHF).

Enzyme assays

THF-dependent cleavage of L-Ser to Gly was monitored using L-[3–^{14}C]-Ser and THF as substrates [34]. THF-independent aldol cleavage of L-*allo*-Thr to Gly and acetaldehyde was measured by estimating (at 340 nm) the rate of NADH-dependent reduction of acetaldehyde to ethanol and NAD^+ catalyzed by alcohol dehydrogenase present in an excess amount in the reaction mixture [4]. The NADH consumed in the reaction was calculated using a molar extinction coefficient of 6220 $M^{-1}\cdot cm^{-1}$. The kinetic constants were calculated using double reciprocal plots. One unit of enzyme activity was defined as the amount of the enzyme that oxidizes one μmol of $NADH\cdot min^{-1}\cdot mg^{-1}$ at 37 °C.

Spectroscopic experiments

Absorption spectra

Changes in the absorption spectra of bsSHMT and E53QbsSHMT resulting from the addition of Gly, L-Ser, THF and FTHF at 20 ± 3 °C were monitored using a Shimadzu (Kyoto, Japan) UV-160 Spectrophotometer. All enzyme concentrations were expressed as mol per subunit.

Steady state kinetic studies

Double reciprocal plots for the formation of quinonoid intermediate before and after dialysis was determined by recording increase in absorbance at 500 nm in Shimadzu UV-160 Spectrophotometer. The enzyme (1 mg) was

incubated with 10 mM glycine and different concentrations of FTHF (0–400 μM) for 1 min and absorbance was measured at 500 nm. The reciprocal of A_{500} was plotted against the corresponding reciprocal of FTHF concentration [18].

The K_d of FTHF for bsSHMT-Gly and E53QbsSHMT-Gly was determined from double reciprocal plots of the change in A_{500} versus FTHF concentration at different fixed concentrations of Gly. A replot of the *y*-intercept versus concentration of Gly gave the K_d values for FTHF. A similar experimental approach was used to determine the K_d in the case of rcSHMT [17,35].

CD spectra

CD measurements were made using a Jasco (Tokyo, Japan) J-500 A automated recording spectropolarimeter. Spectra were collected at a scan speed of 20 nm per min and a response time of 16 s. The CD spectra obtained were plotted as molar ellipticity (θ_{ME}) assuming a subunit MW of 45 kDa for the enzyme.

$$\theta_{ME} = (\theta \times 100 \times MW)/cd$$

Where θ = observed ellipticity (°), c = concentration of protein in mg·ml^{-1} and d = path length in decimeter (0.01 nm). Visible CD spectra were recorded from 500–300 nm using 1 mg·mL^{-1} protein in the presence of L-Ser, Gly, THF and FTHF.

Stopped-flow spectrophotometry

The presteady state kinetics of wild-type and the mutant enzymes with Gly or Gly and THF/FTHF were monitored using a SX.18MV-R stopped-flow spectrophotometer (Applied Photophysics Ltd., Leatherhead, UK) with a path length of 2 mm and a pressure of 125 psi (compressed nitrogen). The dead time of the instrument was 10 ms.

All experiments were performed in 50 mM potassium phosphate pH 7.4 containing 1 mM EDTA and 1 mM 2-mercaptoethanol. Single wavelength stopped-flow kinetic measurements were performed at 25 °C maintained by a circulating water bath. The components were mixed using two syringes, one containing the enzyme (500 μM) and the other containing Gly (100 mM) or Gly and THF (70 μM) or Gly and FTHF (200 μM). The contents were mixed and the reaction was initiated. Single wavelength data were collected at different time regimes. For each data set, 1000 data points were collected. All experiments were repeated at least three times. The data were analyzed using SX.18MV-R, version 4.42 [36,37].

Estimation of PLP at the active site

The enzyme (1 mg·mL^{-1}) was incubated with 0.1 M NaOH for 5 min and the absorption spectra were recorded in the range 300–550 nm. The PLP content was determined by using a molar absorption coefficient value for PLP (6600 M^{-1}·cm^{-1} at 388 nm).

Thermal denaturation studies

The thermal denaturation of bsSHMT and the E53QbsSHMT in the absence and presence of ligands, such as L-Ser and Gly were carried out by measuring the absorbance changes at 287 nm in a Jasco V-530 UV-VIS spectrophotometer. The protein (300 μL of 0.3 mg), with or without the ligand, was taken, with appropriate blanks, in thermal quartz cuvettes and equilibrated at 30 °C to obtain the baseline. The samples were heated from 30 °C to 90 °C at the rate of 1 °C·min^{-1} using a programmable thermal control unit. The absorbance change in each case was monitored at 287 nm and the values were averaged from two independent experiments. The first derivative of the denaturation profile was used to evaluate the apparent T_m using the software supplied with the instrument. The results were analyzed according to the method of White and Olsen [38] in which the fraction of the protein in the denatured state (F_D) is given by:

$$F_D = A_T - A_N/A_D - A_N$$

Where A_N is the absorbance of the protein sample at 30 °C, A_D is the absorbance of the sample at 80 °C and A_T is the absorbance of the protein sample at different temperatures between 30 °C and 80 °C. The apparent T_m was defined as the temperature at which the value of F_D was 0.5.

Acknowledgements

MRNM and HSS thank the Indian Council of Medical Research and the Department of Biotechnology (DBT) of the Government of India for financial support. Diffraction data were collected at the X-ray facility for Structural Biology at the Molecular Biophysics Unit, Indian Institute of Science, supported by the Department of Science and Technology and DBT. We thank Babu and James for their help during data collection. VR and BSB thank the Council for Scientific and Industrial Research, Government of India, for the award of fellowships.

References

1 Mehta PK & Christen P (2000) The molecular evolution of pyridoxal-5′-phosphate-dependent enzymes. *Adv Enzymol Relat Areas Mol Biol* **74**, 129–184.
2 Matthews RB & Drummond JT (1990) Providing one-carbon units for biological methylations: mechanistic studies on the serine hydroxymethyltranferase, methylenetetrahydrofolate reductase and

methylthetrahydrofolate-homocysteine methyltransferase. *Chem Rev* **90**, 1275–1290.
3 Appaji Rao N, Talwar R & Savithri HS (2000) Molecular organization, catalytic mechanism and function of serine hydroxymethyltransferase – a potential target for cancer chemotherapy. *Int J Biochem Cell Biol* **32**, 405–416.
4 Malkin LI & Greenberg DM (1964) Purification and properties of threonine or *allo*-threonine aldolase from rat liver. *Biochim Biophys Acta* **85**, 117–131.
5 Chen MS & Schirch LV (1973) Serine transhydroxymethylase. A kinetic study of the synthesis of serine in the absence of tetrahydrofolate. *J Biol Chem* **248**, 3631–3635.
6 Ulevitch RJ & Kallen RG (1977) Purification and characterization of pyridoxal 5′-phosphate dependent serine hydroxymethylase from lamb liver and its action upon beta-phenylserines. *Biochemistry* **16**, 5342–5350.
7 Schirch V (1998) *Compherensive Biological Catalysis: A Mechanistic Reference*, pp. 211–272. Academic Press Ltd, San Diego, CA.
8 Renwick SB, Snell K & Baumann U (1998) The crystal structure of human cytosolic serine hydroxymethyltransferase: a target for cancer chemotherapy. *Structure* **6**, 1105–1116.
9 Szebenyi DM, Liu X, Kriksunov IA, Stover PJ & Thiel DJ (2000) Structure of a murine cytoplasmic serine hydroxymethyltransferase quinonoid ternary complex: evidence for asymmetric obligate dimers. *Biochemistry* **39**, 13313–13323.
10 Scarsdale JN, Kazanina G, Radaev S, Schirch V & Wright HT (1999) Crystal structure of rabbit cytosolic serine hydroxymethyltransferase at 2.8 Å resolution: mechanistic implications. *Biochemistry* **38**, 8347–8358.
11 Scarsdale JN, Radaev S, Kazanina G, Schirch V & Wright HT (2000) Crystal structure at 2.4 Å resolution of *E. coli* serine hydroxymethyltransferase in complex with glycine substrate and 5-formyl tetrahydrofolate. *J Mol Biol* **296**, 155–168.
12 Trivedi V, Gupta A, Jala VR, Saravanan P, Rao GS, Rao NA, Savithri HS & Subramanya HS (2002) Crystal structure of binary and ternary complexes of serine hydroxymethyltransferase from *Bacillus stearothermophilus*: insights into the catalytic mechanism. *J Biol Chem* **277**, 17161–17169.
13 Schirch D, Delle Fratte S, Iurescia S, Angelaccio S, Contestabile R, Bossa F & Schirch V (1993) Function of the active-site lysine in *Escherichia coli* serine hydroxymethyltransferase. *J Biol Chem* **268**, 23132–23138.
14 Jagath JR, Sharma B, Rao NA & Savithri HS (1997) The role of His-134-147, and -150 residues in subunit assembly, cofactor binding, and catalysis of sheep liver cytosolic serine hydroxymethyltransferase. *J Biol Chem* **272**, 24355–24362.
15 Szebenyi DM, Musayev FN, di Salvo ML, Safo MK & Schirch V (2004) Serine hydroxymethyltransferase: role of glu75 and evidence that serine is cleaved by a retroaldol mechanism. *Biochemistry* **43**, 6865–6876.
16 Jala VR, Prakash V, Rao NA & Savithri HS (2002) Overexpression and characterization of dimeric and tetrameric forms of recombinant serine hydroxymethyltransferase from *Bacillus stearothermophilus*. *J Biosci* **27**, 233–242.
17 Schirch L & Ropp M (1967) Serine transhydroxymethylase. Affinity of tetrahydrofolate compounds for the enzyme and enzyme–glycine complex. *Biochemistry* **6**, 253–257.
18 Katz M & Westley J (1979) Enzymic memory. Steady state kinetic and physical studies with ascorbate oxidase and aspartate aminotransferase. *J Biol Chem* **254**, 9142–9147.
19 Jean B, Jacques R & Jean-Claude M (1977) Enzyme memory: kinetics and thermodynamics of the slow conformation changes of wheat-germ hexokinase LI. *Eur J Biochem* **80**, 593–601.
20 Meunier JC, Buc J & Ricard J (1979) Enzyme memory. Effect of glucose 6-phosphate and temperature on the molecular transition of wheat-germ hexokinase LI. *Eur J Biochem* **97**, 573–583.
21 Yennawar HP, Yennawar NH, Farber GK (1995) A structural explanation for enzyme memory in nonaqueous solvents. *J Am Chem Soc* **117**, 577–585.
22 Alexander MK (1995) What is remembered and why? *Nature* **374**, 596.
23 Studier FW & Moffatt BA (1986) Use of bacteriophage T7 RNA polymerase to direct selective high-level expression of cloned genes. *J Mol Biol* **189**, 113–130.
24 Sambrook J, Fritsch EF & Maniatis T (1989) *Molecular Cloning: A Laboratory Manual*, 2nd edn. Cold Spring Harbor Laboratory, Cold Spring Harbor, NY.
25 Alexander DC (1987) An efficient vector-primer cDNA cloning system: large scale preparation of competent cells. *Meth Enzymol* **154**, 41–64.
26 Lowry OH, Rosebrough NJ, Farr AL & Randall RJ (1951) Protein measurement with the Folin phenol reagent. *J Biol Chem* **193**, 265–275.
27 Otwinowsky ZM & W (1997) Processing of X-ray diffraction data collected in oscillation mode. *Meth Enzymol* **276**, 307–326.
28 Murshudov GN, Vagin AA & Dodson EJ (1997) Refinement of macromolecular structures by the maximum-likelihood method. *Acta Crystallogr D Biol Crystallogr* **53**, 240–255.
29 Emsley P & Cowtan K (2004) Coot: model-building tools for molecular graphics. *Acta Crystallogr D Biol Crystallogr* **60**, 2126–2132.
30 Laskowski RA, McArthur MW, Moss DS & Thornton JM (1993) PROCHECK: a program to check the stereo-chemical quality of protein structures. *J Appl Crystallogr* **26**, 283–291.

31 DeLano WL (2002) *The PYMOL Molecular Graphics System*. DeLano Scientific, San Carlos, CA.
32 Holm L & Sander C (1993) Protein structure comparison by alignment of distance matrices. *J Mol Biol* **233**, 123–138.
33 Hodel A, Kim S & Brunger AT (1992) Model bias in macromolecular crystal structures. *Acta Cryst* **A48**, 851–858.
34 Taylor RT & Weissbach H (1965) A radioactive assay for serine hydroxymethyltransferase. *Anal Biochem* **13**, 80–84.
35 Stover P & Schirch V (1991) 5-Formyltetrahydrofolate polyglutamates are slow tight binding inhibitors of serine hydroxymethyltransferase. *J Biol Chem* **266**, 1543–1550.
36 Baskaran N, Prakash V, Appu Rao AG, Radhakrishnan AN, Savithri HS & Appaji Rao N (1989) Mechanism of interaction of O-amino-D-serine with sheep liver serine hydroxymethyltransferase. *Biochemistry* **28**, 9607–9612.
37 Acharya JK, Prakash V, Rao AG, Savithri HS & Rao NA (1991) Interactions of methoxyamine with pyridoxal-5′-phosphate-Schiff's base at the active site of sheep liver serine hydroxymethyltransferase. *Indian J Biochem Biophys* **28**, 381–388.
38 White FL & Olsen KW (1987) Effects of cross linking on the thermal stability of hemoglobin. *Arch Biochem Biophys* **258**, 51–57.